Revision 2

An integrated EPMA-EBSD study of metamorphic histories recorded in garnet

MASAKI ENAMI[1, 2*], TAKAYOSHI NAGAYA[3, 4] AND MAW MAW WIN[3, 5]

[1] Center for Chronological Research, Nagoya University, Nagoya 464-8602, Japan

[2] Present address: Institute for Space-Earth Environmental Research, Nagoya University, Nagoya 464-8601, Japan

[3] Department of Earth and Planetary Sciences, Graduate School of Environmental Studies, Nagoya University, Nagoya 464-8601, Japan

[4] Present address: Department of Environmental Studies for Advanced Society, Graduate School of Environmental Studies, Tohoku University, Sendai 980-8579, Japan

[5] Present address: Yadanabon University, Amarapura, Mandalay, Myanmar

* E-mail: enami@nagoya-u.jp

ABSTRACT

Growth histories recorded in garnet grains in metasedimentary rocks from the Sanbagawa belt in Japan and the Mogok belt in Myanmar were analyzed using an effective combination of electron backscatter diffraction (EBSD) and electron-probe microanalysis (EPMA) data. Garnet in the Sanbagawa metapelite has inner and outer zones that formed in the eclogite and epidote–amphibolite facies stages, respectively. Based on EPMA element mapping, this garnet appears to have grown as a single crystal with a temporal break in growth between the inner and outer zones that occurred during exhumation. The EBSD data, however, document that the garnet grain is composed of four domains. The misorientation angles of crystallographic orientations between the domains are as large as 59°, and domain boundaries crosscut the growth zoning and the compositional boundary between the inner and outer zones. Sets of quartz grains included in the garnets on either side of the domain boundaries sometimes share the same crystallographic orientation with misorientation angles less than 4°. The garnet grains formed via a 3-step process of prograde crystallization of polycrystalline garnet during the eclogite facies stage (inner zone) → resorption around garnet rims and along domain boundaries during exhumation → crystallization of the outer zone and in the domain boundaries during the prograde epidote–amphibolite facies stage.

The garnet porphyroblasts in the Mogok pelitic gneisses, which formed during prograde metamorphism to the upper amphibolite–granulite facies (0.6–1.0 GPa/780–850°C), are now separated into segments of various sizes by mosaic or symplectite aggregates of biotite, plagioclase, and quartz or monomineralic biotite veins. The segment texture formed at about 0.3–0.4 GPa/610–650°C or lower-grade conditions. The EBSD analysis shows that most of the segments share the same crystallographic

orientation with misorientation angles less than 4° and show no evidence of deformation and/or rotation processes after segmentation. These data suggest that the Mogok sample did not experience dynamic deformation of the garnet grains after the resorption and segmentation stage and may have been exhumed under static conditions from depths of 9–12 km.

Keywords: EBSD, EPMA, garnet, polycrystals, growth process, metamorphism

INTRODUCTION

Garnet grains serve as an important time capsule by recording the metamorphic evolution of their host rock. Pioneering work by Banno (1965), using electron-probe microanalysis (EPMA), showed compositional heterogeneity of garnet grains in Sanbagawa metapelites and concluded that prograde garnet grains commonly have bell-shaped Mn zoning and are not in complete equilibrium with other matrix phases during prograde metamorphism. Thompson et al. (1977) correlated compositional zoning in garnet with the nature and distribution of its inclusions in the Gassetts schist from Vermont to reveal the paragenetic history of rocks from upper greenschist to lower amphibolite facies conditions. This might have been one of the earliest efforts to exploit the mineralogical characteristics of garnet for interpretation of metamorphic pressure (*P*)–temperature (*T*) paths, and is a concept that has been extensively developed ever since. Moreover, pioneering work by Fliervoet et al. (1997) on deformation (*D*) mechanisms in ultramylonites from the Redbank Deformed Zone, Central Australia, recognized electron backscatter diffraction (EBSD) as an important tool in the analysis of garnet growth.

Garnet generally shows concentric bell-shaped Mn-zoning, which is considered to be formed by nucleation and subsequent continuous growth. Single garnet grains, however, sometimes exhibit multiple regions of high Mn content, which is considered to represent discrete garnet nuclei and their coalescence to form a large porphyroblast (e.g., Spiess et al. 2001; Okamoto and Michibayashi 2006). In contrast, Hirsch et al. (2003), using EBSD, quantitatively measured the crystallographic orientation of garnet porphyroblasts with multiple domains of Mn-zoning from Harpswell Neck, Maine, and concluded that they exhibited no variation in crystallographic orientation among

domains. Thus, a new concept for the growth model of a complex-zoned garnet was proposed in which precursor phases rich in Mn were overgrown, and their Mn was incorporated locally into the garnet structure. The combination of EPMA and EBSD analyses have provided key data for evaluating the growth mechanisms of garnet grains with atoll (Cheng et al. 2007; Ruiz Cruz 2011), snowball (Robyr et al. 2007), and lath shapes (Schertl and Neuser 2007) and for elucidating the interaction between deformation and chemical reaction that occurs during metamorphism (Griffiths et al. 2014).

Polycrystalline porphyroblasts of garnet with high-angle misorientation boundaries from various types of metamorphic rocks were described by Whitney et al. (2008) and Whitney and Seaton (2010) who determined that the occurrence of polycrystalline garnet porphyroblasts is more frequent than previously believed. Whitney et al. (2008) grouped polycrystalline garnet grains into two types based on Mn growth zoning. Garnet of the first type has concentric compositional zoning of Mn and appears to be a single crystal. The concentric growth zoning of this type of garnet crosscut by high-angle misorientation boundaries. Garnet of the second type has multiple growth nuclei and is identifiably polycrystalline based on both Mn X-ray mapping and EBSD data. In both types of polycrystalline garnet, inclusions of quartz and ilmenite sometimes occur across the domain boundaries. Whitney et al. (2008) determined that the garnet polycrystals formed continuously during the prograde stage and that the differences in compositional zonings can be largely attributed to the spatial distribution of Mn-rich nuclei, i.e., closely or widely spaced nuclei at the early stage of garnet formation [Fig. 18 of Whitney et al. (2008)]. Whitney and Seaton (2010) further reported a disconnect between Mn–Fe–Mg zoning and Ca zoning relative to the high-angle misorientation

boundaries and proposed the existence of four types of polycrystalline garnet based on the relationships between these two zoning types and high-angle misorientation boundaries [Fig. 11 of Whitney and Seaton (2010)]. These data have prompted important questions in the discussion of metamorphic *P–T* paths based on the relationships between the zonal structure and inclusions of garnet because the center of a zoned garnet does not always represent the earliest stage of garnet growth. In addition, the misorientation boundaries may behave as channels to promote element exchange between the garnet interior and the matrix phases.

Although several important EBSD studies of natural garnet have been conducted, including those listed above, most of these have primarily focused on the growth mechanism of porphyroblasts and deformation processes (e.g., Fliervoet et al. 1997; Prior et al. 2000; Kleinschrodt and Duyster 2002; Storey and Prior 2005; Vollbrecht et al. 2006). Integrated EPMA X-ray mapping and EBSD analysis may also provide important additional information for revealing the *P–T–D* history. For this study, we selected two samples: one from the high-pressure Sanbagawa metamorphic belt, and the second from the high-temperature Mogok metamorphic belt as case studies to investigate the relationships between the compositional and crystallographic characteristics obtained from EMPA X-ray mapping and EBSD analysis and the implications for the metamorphic *P–T–D* paths. The Sanbagawa garnet is considered to have experienced discontinuous growth of inner and outer zones based on the compositional zoning and distribution of inclusions. The results of the EBSD analysis revealed that this garnet is composed of four segments and that its high-angle misorientation boundaries crosscut the boundary between the inner and outer zones, which suggests that the polycrystalline texture resulted from multiple nucleations and

their coalescence during the early stages of garnet crystallization. The Mogok garnet porphyroblasts were separated into several segments via resorption during exhumation. The EBSD data show no significant misorientation among these segments, which implies static conditions during the later stages of exhumation.

GENERAL GEOLOGY OF SAMPLE LOCALITES

The two samples discussed in this paper, UKE07b and S22b, are high-pressure Sanbagawa metamorphic rock from Japan (e.g., Banno and Sakai 1989; Wallis et al. 2000) and high-temperature Mogok metamorphic rock from Myanmar (e.g., Searle et al. 2007), respectively.

Sanbagawa metamorphic rock

The Sanbagawa sample (UKE07b) was collected from the Besshi region of the Sanbagawa metamorphic belt, central Shikoku, Japan, where metapelite and metabasite recrystallized under epidote-amphibolite-facies conditions (Enami 1983; Higashino1990). Common mineral assemblages of the metapelite and metabasite are garnet + biotite + muscovite + chlorite + sodic-calcic amphibole + epidote + sodic plagioclase + quartz + graphite and sodic-calcic amphibole + garnet + muscovite + epidote + chlorite + sodic plagioclase + quartz, respectively. However, eclogitic assemblages such as garnet + omphacite + quartz occur sporadically in the metabasites (Takasu 1984; Aoya 2001; Kugimiya and Takasu 2002; Ota et al. 2004; Miyagi and Takasu 2005; Sakurai and Takasu 2009; Endo 2010) and rarely in the metapelites (Kouketsu and Enami 2010; Kouketsu et al. 2010) of the high-grade zone. Thus, the Besshi region is divided into eclogite- and non-eclogite units (Kouketsu et al. 2014a).

The eclogite-unit lithologies record the relatively complex *P–T* history of the prograde eclogite facies stage → exhumation and hydration stage → prograde epidote–amphibolite facies stage (Fig. 1a). On the contrary, the non-eclogite unit lithologies were recrystallized during simple prograde metamorphism up to the epidote–amphibolite facies. These two units are considered to have been juxtaposed after exhumation of the eclogite unit and before the peak stage of the prograde epidote–amphibolite facies metamorphism. The lithologies of the eclogite and non-eclogite units and their boundary were extensively recrystallized under the prograde epidote–amphibolite facies stage. Therefore, it is difficult to directly observe the tectonic boundary between the two units at the outcrop scale; thus the unit boundaries are usually determined on the basis of the following combinations: (1) sodic-phase inclusions in garnet, (2) residual pressure of quartz inclusion in garnet estimated by quartz Raman barometry (Enami et al. 2007; Kouketsu et al. 2014b), and (3) compositional zoning of garnet (e.g., Mouri and Enami 2008; Sakurai and Takasu 2009; Kouketsu et al. 2014a; Taguchi and Enami 2014) in addition to the occurrences of omphacite-bearing assemblages.

Endo (2010) proposed a clockwise *P–T* path for prograde eclogite facies metamorphism and estimated the conditions as 1.9–2.1 GPa/525–565°C and 1.4–1.6 GPa/635°C for the peak pressure and temperature stages, respectively. The equilibrium conditions of the peak eclogite facies stage varied slightly from 1.8–1.9 GPa/495–530°C to 2.3–2.4 GPa/675–740°C within the eclogite unit (e.g., Ota et al. 2004; Miyamoto et al. 2007; Kabir and Takasu 2010; Kouketsu et al. 2010; Endo and Tsuboi 2013). The *P–T* conditions in the epidote–amphibolite facies stage of the high-grade zone were estimated to be 0.8–1.1 GPa/470–635°C (Enami 1983; Enami et al. 1994;

Wallis et al. 2000).

Mogok metamorphic rock

The Mogok sample (S22b) was collected from the Sagaing area of the Mogok metamorphic belt, Myanmar (cf., Fig. 1c of Maw Maw Win et al. 2016). In the Sagaing area, the Mogok metamorphic rocks are composed mainly of pelitic gneiss, marble, calc–silicate rock, and amphibolite of amphibolite–granulite facies grade (Mitchell et al. 2007; Maw Maw Win et al. 2016). The pelitic gneiss, which is a predominant lithology in the Sagaing area, is composed mainly of garnet, biotite, plagioclase, K-feldspar, quartz, and graphite. The marble and calc–silicate rocks usually contain phlogopite, diopside, forsterite, grossular garnet, and graphite in addition to calcite. The amphibolite contains mainly hornblende, plagioclase, and epidote with small amounts of biotite and titanite. The petrographical characteristics of the Mogok pelitic gneisses in the Sagaing area and the locality of sample S22b have been described by Maw Maw Win et al. (2016). Pressure–temperature conditions at peak metamorphic stage and exhumation and hydration stage were estimated at 0.6–1.0 GPa/780–850°C and 0.3–0.5 GPa/600–680°C, respectively (Fig. 1b).

ANALYTICAL PROCEDURES

Thin sections for X-ray and EBSD mapping analyses and quantitative analyses of major phases were polished by using a series of diamond pastes with decreasing grain sizes down to ¼μm. The X-ray mapping images and the quantitative analyses were conducted by using EPMA with wavelength-dispersive spectrometers (JXA-8900R, JEOL, Tokyo, Japan) at the Petrology Laboratory of Nagoya University. The

accelerating voltage and specimen current on Faraday cup were stabilized at 20 kV and 100 nA and 15 kV and 12 nA for the X-ray mapping and quantitative analyses, respectively. A beam with a diameter of 2–3 μm was used for the garnet and amphibole analyses; analyses of mica and feldspar were made using a 5 μm beam spot. Well-characterized natural and synthetic phases were used to calibrate the instrument. Matrix corrections were performed using the α-factor table of Kato (2005). Iron in analyzed phases other than epidote was assumed to be ferrous. The compositional characteristics of the garnet are discussed using proportions of end-members estimated as those of divalent cations in the eight coordinated sites; e.g., Prp = Mg/(Fe + Mn + Mg + Ca) × 100. Representative analyses of the major minerals in samples UKE07b and S22b are on deposit as Supplemental Table 1[1]. The abbreviations for minerals and end-members used in this paper follow those defined by Whitney and Evans (2010).

For EBSD analysis, the polished thin sections prepared using diamond pastes were additionally treated with colloidal silica for up to 1 h to remove the surface damage. Crystal orientations were determined at Nagoya University using a JEOL JSM-6510LV scanning electron microscope equipped with a Nordlys Nano detector–AZtec (version 2.3) EBSD system at 20 kV accelerating voltage and a working distance of 26–28 mm. The camera binning and Hough resolution were 4 × 4 and 90, respectively. The maximum (minimum) numbers of band detections were 10 (5). The EBSD patterns were collected under a low vacuum of 10 Pa, which allowed the use of uncoated samples (e.g. Padròn-Navarta et al. 2012; Nagaya et al. 2014). Computerized indexing

[1] Deposit item AM-1X-XXX, Supplemental Table. A deposit item is stored on the MSA web site and available via the American Mineralogist Table of Contents. Find the article in the table of contents at GSW (ammin.geoscienceworld.org) or MSA (www.minsocam.org), and then click on the deposit link.

of the diffraction pattern was automatically determined for each measurement. The maximum accepted angular deviation for map measurements was 2.0°. The crystallographic parameters of Novak and Gibbs (1971) and Levien et al. (1980) were employed to index the Kikuchi patterns for garnet, at a = 11.531 Å, and for quartz, at a = 4.916 Å, c = 5.4054 Å, respectively. Software developed by D. Mainprice was used to prepare the pole figures (Mainprice 1990).

X-RAY MAPPING AND EBSD ANALYSIS

UKE07b

The UKE07b metapelite was collected from an outcrop 20–30 m inside the northeastern margin of the eclogite unit (longitude 133°25′24″E and latitude 33°53′43″N). This sample contains garnet, biotite, phengite [Si = 3.30–3.41 per formula unit (pfu) for O = 11], chlorite, epidote [$Y_{Fe} = Fe^{3+}/(Al + Fe^{3+})$ = 0.09–0.11], barroisite–katophorite (Si = 6.66–6.70 pfu, Ca = 1.27–1.34 pfu for O = 23), albite, and quartz with minor amounts of rutile, ilmenite, titanite, apatite, and graphite as matrix phases. The biotite was retrogressively altered to secondary chlorite. Paragonite occurs only as inclusions in the garnet. Garnet grains show rounded and subhedral form. Their grain sizes vary from 100–200 μm to 2–3 mm in diameter, and most of them are coarse-grained of >500 μm. These relatively coarse garnet grains usually show duplex texture consisting of inner and outer zones identified by the distributions of quartz and graphite inclusions visible under a polarizing microscope.

The selected garnet (2.3 mm in size) is also composed of inner and outer zones, visible under the polarizing microscope (Fig. 2a); these results were confirmed by X-ray mapping analyses (Figs. 2b–e). The inner zone is characteristically rich in quartz

and fine-grained paragonite, titanite, rutile, and graphite inclusions. The outer zone contains albite rather than paragonite as sodic-phase inclusion. The boundary between the inner and outer zones is also defined by compositional discontinuity (Figs. 2b–f and 3). The inner zone is relatively homogeneous ($Alm_{67–73}Prp_{4–10}Sps_{3–10}Grs_{16–21}$) with slightly decreasing spessartine and increasing pyrope contents from the core toward the margin. The grossular and spessartine contents discontinuously increase, and almandine and pyrope contents discontinuously decrease at the boundary from the inner to outer zones. In the outer zone, the pyrope content increases and the spessartine content decreases toward the outermost rim ($Alm_{56–66}Prp_{4–9}Sps_{0–10}Grs_{26–36}$). These compositional trends of the inner and outer zones imply prograde formations of these two zones and a discontinuity in garnet growth between the formation stages of the two zones (cf., Fig. 1a). The inner zone contains paragonite and quartz retaining high residual pressure up to 0.6–0.7 GPa, which was thus formed during the eclogite facies stage (cf., Enami et al. 2007; Kouketsu and Enami 2011; Kouketsu et al. 2014a). The outer zone contains albite as inclusions and is a later product than the inner zone, suggesting formation during the epidote–amphibolite facies stage.

X-ray mapping analysis revealed concentric zonal structure in the examined garnet grain that appears to have formed from the crystal core toward the rim. The EBSD analysis, however, shows that the grain is polycrystalline, consisting of four domains separated by high-angle misorientation boundaries at 40°–59° (Figs. 4a and b). These domain boundaries are not related to major element zoning and transect the compositional boundary between the inner and outer zones. Although the quartz inclusions in the garnet grain show no obvious lattice preferred orientation (Figs. 4a and c), those occurring separate from one another across the domain boundaries sometimes

share the same crystallographic orientation (Fig. 5). The misorientation angles between quartz inclusions of sets A (grains 1, 2, and 3), B (4 and 5), and C (6 and 7) are less than 5°, 6°, and 2°, respectively.

S22b

The S22b pelitic gneiss collected from the Shwe Myin Tin valley (longitude 95°59′57′′E and latitude 22°02′12′′N) contains garnet, biotite, plagioclase ($An_{43\pm2}$), K-feldspar, and quartz with minor amounts of rutile, ilmenite, graphite, apatite, monazite, and zircon as matrix phases. Biotite grains are characteristically rich in Ti, and their TiO_2 contents are up to 6.2 wt% in phase included by garnet and 4.9 wt% in matrix phase (Ye Kyaw Thu et al. 2016: in press). Sillimanite occurs only as inclusions in the garnet. Garnet grains are anhedral, and some show unusually elongate shapes with aspect ratios up to 1:5 (Figs. 6a–c). The large and elongate garnet grains contain quartz inclusions in their mantle zones showing poikilitic texture. This sample does not show obvious preferred orientation of biotite in the matrix and pressure shadows around the garnet porphyroblasts. The garnet porphyroblasts were retrogressively re-equilibrated under upper greenschist–lower amphibolite facies conditions and are usually separated into several segments by two-types of replacement texture (Maw Maw Win et al. 2016). The earlier re-equilibrium stage is represented by mosaic or symplectite aggregates of biotite, plagioclase, and quartz around the garnet (Figs. 6a, d, and e). The biotite in the aggregates is usually poorer in TiO_2 (usually 1–3 wt%) than the isolated phase in the matrix (up to 4.9 wt%). The later re-equilibrium product is a monomineralic vein of biotite (Fig. 6), which is poorer in TiO_2 (usually less than 0.3 wt%) than the isolated phase and the aggregate phase in the matrix.

The garnet segments are composed of relatively homogeneous cores ($Alm_{60–63}Prp_{29–33}Sps_1Grs_{5–7}$) and thin Mg-poor and Mn-rich mantles ($Alm_{63–74}Prp_{17–29}Sps_{2–4}Grs_{4–7}$; Figs. 6b–e and 7). In the mantle of grains the pyrope content gradually decreases toward the outermost rim; the almandine and spessartine contents show the opposite trends. The compositional gradient of the mantle part formed along with the segmentation during the retrograde stage, as discussed by Maw Maw Win et al. (2016). Fine-grained garnet sometimes occurs in the aggregates of biotite + plagioclase + quartz and has a chemical composition ($Alm_{70–78}Prp_{13–21}Sps_{2–4}Grs_{4–7}$) similar to the outermost rim of the garnet. Thus, the Mn-rich garnet + biotite + plagioclase + quartz assemblage likely represents the equilibrium reached when the garnet grains were segmented, as discussed by Maw Maw Win et al. (2016). The local modification in composition of garnet around the monomineralic biotite veins is less extensive than that in the grain mantles (Figs. 6b–e). The anorthite contents of plagioclase are not critically different between the isolated phase in matrix ($An_{43±2}$) and the aggregate phase ($An_{41 ± 4}$).

The garnet segments in the area analyzed by EBSD were grouped into three sets of 1–8, 9–12, and 13–15, which are hereafter referred to as garnet sets 1, 2, and 3, respectively (Figs. 8a and d). Garnet sets 1 and 3 contain abundant fine-grained needles of sillimanite, and the garnet set 2 is poor in sillimanite and other inclusions. The differences in the modal amounts of inclusions and the alignment patterns of the sillimanite inclusions imply that the three sets of garnet were likely derived from three different grains (Fig. 6a). The segments of garnet sets 1 and 3 are separated by monomineralic biotite veins except for the cases between segments 1 and 2 and segments 13 and 14, which are bounded by mosaic aggregates of biotite, plagioclase, and quartz. In garnet set 1, the misorientation angles between segments 2 and 8, which

are adjacent, are less than 4°; that misorientation between segments 1 and 2 is 14° (Figs. 8a and b). Segments 14 and 15 of garnet set 3, which are bounded by biotite veins, are misoriented by less than 1°, and the misorientation angle between segments 13 and 14 is 62° (Figs. 8d and e). Garnet set 2 is composed of four segments separated by mosaic aggregates. Segments 9–11 share similar crystallographic orientations, with misorientation angles of less than 4°; segment 12 has high-angle misorientation angles of 33° relative to other segments (Figs. 8a and c).

DISCUSSION

Discontinuous growth of polycrystalline garnets in the Sanbagawa metapelite

Two petrographical characteristics—the relationship between the compositional zoning and domain structure and the crystallographic orientation of quartz inclusions in the garnet—are critical for discussing the growth process of the UKE07b garnet and metamorphic *P–T* history of the Sanbagawa belt. The Sanbagawa garnet is polycrystalline, and their domain boundaries are developed independent of the compositional growth zoning (Figs. 2b and 4a). This relationship is similar to the case of concentric zoned garnet polycrystals reported by Whitney et al. (2008) and Whitney and Seaton (2010). The Sanbagawa garnet, however, experienced two stages of prograde metamorphism and records the discontinuance of crystal growth between them (Fig. 1a). In addition, the quartz grains included on each side of the garnet domain boundary of the inner zone frequently share similar crystallographic orientation with misorientation angles less than 2–6° (Fig. 5). The presence of quartz inclusions sharing similar crystallographic orientation along the domain boundary disproves the interpretation that the polycrystalline garnet and high-angle boundaries were formed by

deformation and rotation mechanisms after formation of the porphyroblast. Whitney et al. (2008) studied polycrystalline garnet in mica schist from Townshend Dam and reported that inclusions along the high-angle boundaries in polycrystalline garnet were not offset; thus, they argued that deformation and rotation mechanisms did not cause the formation of the polycrystalline garnet. Our observations suggest that the polycrystalline garnet in sample UKE07b was formed by a process similar to that discussed by Whitney et al. (2008).

Higher resolution X-ray element mapping around the domain boundaries (10–20 μm in width) shows local modification of the compositions along the boundaries (Figs. 2c, e, and f). The compositionally modified zone connects to the boundary between the inner and outer zones (Fig. 2f). The compositional ranges of the garnet between the quartz grains (Areas A–C, Figs. 5a and c) and around the domain boundary (Area D, Fig. 5c) are $Alm_{67–72}Prp_{5–10}Sps_{3–6}Grs_{16–22}$, which are similar to those between the outermost part of the inner zone and the innermost part of the outer zone (Fig. 9). These features suggest the occurrence of two processes: (1) resorption of the garnet's inner zone and quartz inclusions along the domain boundaries by hydration reactions after infiltration of metamorphic fluid during exhumation and a probable temperature decrease and (2) their sealing by neo-crystallization of garnet during the subsequent prograde stage under epidote–amphibolite facies conditions.

Figure 10 illustrates conceptual diagrams of the garnet nucleation and growth scenario in the case of the Sanbagawa garnet inferred from the EMPA and EBSD data . Considering that the *P–T* trajectory of the Sanbagawa eclogite facies rocks have two stages of prograde metamorphism (Fig. 1a), the formation process of the polycrystalline garnet is summarized in the following five processes: (1) formation of closely spaced

nuclei of garnet, their coalescence, and trapping of quartz crystals at their domain interface similar to the case of Fig. 18a of Whitney et al. (2008); (2) continuous growth during the prograde eclogite facies stage including the formation of the inner zone containing inclusions of quartz and other phases; (3) resorption around the inner zone of the garnet and along its domain boundaries in the exhumation and hydration stage; (4) resurgence of crystallization and sealing of the domain boundaries at the start of the second prograde metamorphism; and (5) continuous growth of the garnet during the prograde epidote–amphibolite facies stage in the formation of the outer zone.

Static exhumation of high-temperature Mogok metamorphic rock

The garnet porphyroblasts in the Mogok metamorphic rocks (S22b) were separated into several segments by mosaic or symplectite aggregates and monomineralic biotite veins. Garnet sets 1 and 3 contain both types of segments bordered by mosaic aggregates and monomineralic veins (Fig. 6). In these garnet sets, the segments separated by monomineralic veins share common crystallographic orientations. On the contrary, segments 1 and 13, which are bordered by mosaic aggregates, show misorientation angles of 14° and 62° to the adjacent segments, respectively (Fig. 8). The high-angle misorientations in segments of sets 1 and 3 might be attributable to two models: (1) primary porphyroblasts with other adjacent segments that were locally rotated after segmentation or (2) independent grains from the other segments that had originally different crystallographic orientations. Although there is little information for discussion of which concept is more plausible, the garnet sets of 1 and 3 (Figs. 8b and e) clearly suggest that the garnet grains did not experience deformation by rotation of these segments after segmentation by monomineralic biotite veins.

Segments 9–12 in garnet set 2 are separated by biotite-bearing mosaic aggregates, with segments 9–11 sharing the same crystallographic orientation. On the contrary, segment 12 shows a misorientation angle of 33° to the adjacent segments. No information is available to rule out the possibility that segment 12 originally formed a porphyroblast with segments 9–11 and the high-angle misorientation indicates local rotation of the segment 12 after their segmentation. However, it is highly probable that segments 9-11 did not experience significant rotation and deformation after their separation. These interpretations might be supported by the fact that pelitic gneiss S22b shows no obvious pressure shadow and local overprinting of the foliation around the garnet porphyroblasts.

The observation of the sets of garnet segments separated by monomineralic biotite veins, i.e. segments 2–8 and 14–15, certainly suggests that the Mogok sample was static during and after the formation of the veins and not in a strain field. Additionally, the set of segments 9–11, which were separated by biotite-bearing mosaic aggregates, shows that the static environments likely began, at the latest, just before or during the formation stage of the mosaic aggregates. The *P–T* conditions during the formation of the biotite-bearing mosaic or symplectite aggregates in segments 9, 10, and 11 were estimated to be 0.3–0.4 GPa/610–650°C (garnet–biotite–plagioclase–quartz (GBPQ) geobarometry (Wu et al. 2004) and garnet–biotite (Grt–Bt) geothermometry (Bhattacharya et al. 1992; Holdaway 2000)). Such formation conditions of the aggregates are consistent with those of other Mogok pelitic gneisses (0.3–0.5 GPa/600–680°C) reported by Maw Maw Win et al. (2016) (Fig. 1b) and the temperature conditions of about 400–500°C estimated for the garnet isograd in medium P/T type metamorphic belts such as the Barrovian zone (e.g., Spear and Cheney 1989; Spear et al.

1990). The garnet porphyroblasts likely segmented under the lower-amphibolite facies conditions. Although the available data is limited to the studied sample, the Mogok sample S22b may have been exhumed from depths of about 9–12 km, without incurring any specific deformation and rotation,

IMPLICATIONS

The combination of EBSD and EPMA analyses discussed in this paper revealed important information on the geological and tectonic developments of Sanbagawa and Mogok metamorphic rocks along with the growth mechanism of metamorphic garnet grains.

Sanbagawa metapelite: Two distinct models have been proposed concerning the *P–T* evolution of the Sanbagawa metamorphic rocks. Aoya (2001), Zaw Win Ko et al. (2005), and Kouketsu et al. (2014a) proposed that the Sanbagawa belt is divided into eclogite and non-eclogite units, and the lithologies of the eclogite unit recording two stages of prograde metamorphism under the eclogite and subsequent epidote–amphibolite facies conditions, as shown in Fig. 1a. As discussed above, this *P–T* history effectively explains the deduced formation mechanism of the polycrystalline garnet porphyroblast in a Sambagawa metapelite (UKE07b) from the eclogite unit. On the contrary, Ota et al. (2004) and Aoki et al. (2009) proposed an alternative concept such that eclogite and associated high-grade rocks record simple *P–T* trajectory with monotonous decreases of *P–T* conditions during exhumation. They considered that the regional thermal structure up to the epidote–amphibolite facies grade in the Sanbagawa belt is not attributed to progressive metamorphism and instead records Barrovian-type overprinting that occurred during exhumation. However, the proposed simple clockwise

P–T path model (Ota et al. 2004; Aoki et al. 2009) does not effectively explain the resorption and subsequent crystallization processes during the eclogite facies and epidote–amphibolite facies stages retained by the Sanbagawa garnet.

Mogok pelitic gneiss: The EBSD and EPMA analyses suggested that the Mogok sample S22b did not record any specific deformation and rotation processes under lower-amphibolite facies and lower-grade conditions during exhumation. There may be two possible interpretations for the record of static condition. One is that the degree of deformation, which the Mogok metamorphic belt experienced during later stages of exhumation, was distinctly heterogeneous throughout the Mogok metamorphic belt, and some outcrops, including sample S22b, were thus locally spared from the impact of the exhumation movement.

The alternative interpretation is that the Mogok metamorphic belt was almost entirely under static conditions during later stages of exhumation. The Mogok metamorphic rocks may be traced to the north at the eastern Himalayan syntaxis (Barley et al. 2003; Licht et al. 2013). Kaneko (1997) tectonically and petrologically studied the Himalayan metamorphic belt, central Nepal, and proposed a two-step exhumation model of the metamorphic rocks. This model consists of semi-adiabatic extrusion from the Moho depth into the mid-crustal level (about 0.4 GPa/600°C) and subsequent doming uplift along with surface denudation. The static exhumation retained by the Mogok garnet might be explained by the erosion and doming uplift process occurring at depths of at least 10 km and is consistent with the tectonic model proposed by Kaneko (1997). Extensive and systematic studies of the Mogok and/or Himalaya metamorphic belts employing EBSD and EPMA methods possibly provide convincing arguments to the

most probable interpretation.

The case studies on the Sanbagawa and Mogok metamorphic rocks suggest that the combination of EBSD and EPMA analyses is a powerful and effective method for studies of the *P–T–D* evolution of metamorphic rocks.

ACKNOWLEDGEMENTS

Valuable and constructive comments by D. L. Whitney, T. A. Griffiths and C. Hetherington greatly helped to improve this manuscript. We thank D. Mainprice for providing the software to analyze the EBSD data. This research was partially supported by Grant-in-Aids for Scientific Research (ME, 25400511; TN, 13J00199 and 16J01480) from the Japan Society for the Promotion of Science (JSPS) and a scholarship (MMW) from Ministry of Education, Culture, Sports, Science and Technology in Japan (MEXT).

REFERENCES CITED

Aoki, K., Kitajima, K., Masago, H., Nishizawa, M., Terabayashi, M., Omori, S., Yokoyama, T., Takahata, N., Sano, Y., and Maruyama, S. (2009) Metamorphic P–T–time history of the Sanbagawa Belt in central Shikoku, Japan and implications for retrograde metamorphism during exhumation. Lithos, 113, 393-407.

Aoya, M. (2001) P–T–D path of eclogite from the Sambagawa belt deduced from combination of petrological and microstructural analyses. Journal of Petrology, 42, 1225-1248.

Banno, S. (1965) Notes on rock-forming minerals (34) Zonal structure of pyralspite garnet in Sanbagawa schists in the Bessi area, Sikoku. Journal of Geological Society of Japan, 71, 185-188.

Banno, S. and Sakai, C. (1989) Geology and metamorphic evolution of the Sanbagawa metamorphic belt, Japan. In J.S. Daly, R.A. Cliff, and B.W.D. Yardley Eds., The Evolution of Metamorphic Belts, 43, p. 519-532. Blackwell Scientific Publications, Oxford.

Barley, M.E., Pickard, A.L., Khin Zaw, Rak, P., and Doyle, M.G. (2003) Jurassic to Miocene magmatism and metamorphism in the Mogok metamorphic belt and the India-Eurasia collision in Myanmar. Tectonics, 22.

Bhattacharya, A., Mohanty, L., Maji, A., Sen, S.K., and Raith, M. (1992) Non-ideal mixing in the phlogopite-annite binary: constraints from experimental data on Mg-Fe partitioning and a reformulation of the biotite-garnet geothermometer. Contributions to Mineralogy and Petrology, 111, 87-93.

Cheng, H., Nakamura, E., Kobayashi, K., and Zhou, Z. (2007) Origin of atoll garnets in

eclogites and implications for the redistribution of trace elements during slab exhumation in a continental subduction zone. American Mineralogist, 92, 1119-1129.

Enami, M. (1983) Petrology of pelitic schists in the oligoclase-biotite zone of the Sanbagawa metamorphic terrain, Japan: phase equilibria in the highest grade zone of a high-pressure intermediate type of metamorphic belt. Journal of Metamorphic Geology, 1, 141-161.

Enami, M., Nishiyama, T., and Mouri, T. (2007) Laser Raman microspectrometry of metamorphic quartz: A simple method for comparison of metamorphic pressures. American Mineralogist, 92, 1303-1315.

Enami, M., Wallis, S.R., and Banno, Y. (1994) Paragenesis of sodic pyroxene-bearing quartz schists: implications for the P-T history of the Sanbagawa belt. Contributions to Mineralogy and Petrology, 116, 182-198.

Endo, S. (2010) Pressure-temperature history of titanite-bearing eclogite from the Western Iratsu body, Sanbagawa metamorphic belt, Japan. Island Arc, 19, 313-335.

Endo, S., and Tsuboi, M. (2013) Petrogenesis and implications of jadeite-bearing kyanite eclogite from the Sanbagawa belt (SW Japan). Journal of Metamorphic Geology, 31, 647-661.

Fliervoet, T.F., White, S.H., and Drury, M.R. (1997) Evidence for dominant grain-boundary sliding deformation in greenschist- and amphibolite-grade polymineralic ultramylonites from the Redbank Deformed Zone, Central Australia. Journal of Structural Geology, 19, 1495-1520.

Griffiths, T.A., Habler, G., Rhede, D., Wirth, R., Ram, F., and Abart, R. (2014)

Localization of submicron inclusion re-equilibration at healed fractures in host garnet. Contributions to Mineralogy and Petrology, 168.

Higashino, T. (1990) The higher-grade metamorphic zonation of the Sambagawa metamorphic belt in central Shikoku, Japan. Journal of Metamorphic Geology, 8, 413-423.

Hirsch, D.M., Prior, D.J., and Carlson, W.D. (2003) An overgrowth model to explain multiple, dispersed high-Mn regions in the cores of garnet porphyroblasts. American Mineralogist, 88, 131-141.

Holdaway, M.J. (2000) Application of new experimental and garnet Margules data to the garnet-biotite geothermometer. American Mineralogist, 85, 881-892.

Kaneko, Y. (1997) Two-step exhumation model of the Himalayan metamorphic belt, central Nepal. Journal of Geological Sociery of Japan, 103, 203-226.

Kabir, M.F. and Takasu, A. (2010) Evidence for multiple burial–partial exhumation cycles from the Onodani eclogites in the Sambagawa metamorphic belt, central Shikoku, Japan. Journal of Metamorphic Geology, 28, 873-893.

Kato, T. (2005) New accurate Bence-Albee α-factors for oxides and silicates calculated from the PAP correction procedure. Geostandrds and Geoanalytical Research, 29, 83-94.

Kleinschrodt, R., and Duyster, J.P. (2002) HT-deformation of garnet: an EBSD study on granulites from Sri Lanka, India and the Ivrea Zone. Journal of Structural Geology, 24, 1829-1844.

Kouketsu, Y., and Enami, M. (2010) Aragonite and omphacite-bearing metapelite from Besshi region, Sambagawa belt in central Shikoku, Japan and its implication. Island Arc, 19, 165-176.

Kouketsu, Y., and Enami, M. (2011) Calculated stabilities of sodic phases in the Sambagawa metapelites and their implications. Journal of Metamorphic Geology, 29, 301-316.

Kouketsu, Y., Enami, M., and Mizukami, T. (2010) Omphacite-bearing metapelite from the Besshi region, Sambagawa metamorphic belt, Japan: Prograde eclogite facies metamorphism recorded in metasediment. Journal of Mineralogical and Petrological Sciences, 105, 9-19.

Kouketsu, Y., Enami, M., Mouri, T., Okamura, M., and Sakurai, T. (2014a) Composite metamorphic history recorded in garnet porphyroblasts of Sambagawa metasediments in the Besshi region, central Shikoku, Southwest Japan. Island Arc, 23, 263-280.

Kouketsu, Y., Nishiyama, T., Ikeda, T., and Enami, M. (2014b) Evaluation of residual pressure in host-inclusion system using the negative frequency shift of quartz Raman spectrum. American Mineralogist, 99, 433-442.

Kugimiya, Y., and Takasu, A. (2002) Geology of the Western Iratsu mass within the tectonic melange zone in the Sambagawa metamorphic belt, Besshi district, central Shikoku, Japan. Journal of Geological Society of Japan, 108, 644-662 (in Japanese with English abstract).

Levien, L., Prewitt , C.T., and Weidner, D.J. (1980) Structure and elasticproperties of quartz at pressure. American Midland Naturalist, 65, 920-930.

Licht, A., France-Lanord, C., Reisberg, L., Fontaine, C., Soe, A.N., and Jaeger, J.J. (2013) A palaeo Tibet-Myanmar connection? Reconstructing the Late Eocene drainage system of central Myanmar using a multi-proxy approach. Journal of Geological Society, London, 170, 929-939.

Mainprice, D.A. (1990) Fortran program to calculate seismic anisotropy from the lattice preferred orientation of minerals. Computers & Geosciences, 16, 385-393.

Maw Maw Win, Enami, M., and Kato, T. (2016) Metamorphic conditions and CHIME monazite ages of Late Eocene to Late Oligocene high-temperature Mogok metamorphic rocks in central Myanmar. Journal of Asian Earth Sciences, 117, 304-316.

Mitchell, A.H.G., Myint Thein Htay, Kyaw Min Htun, Myint Naing Win, Thura Oo, and Tin Hlaing. (2007) Rock relationships in the Mogok metamorphic belt, Tatkon to Mandalay, central Myanmar. Journal of Asian Earth Sciences, 29, 891-910.

Miyagi, Y., and Takasu, A. (2005) Prograde eclogites from the Tonaru epidote amphibolite mass in the Sambagawa Metamorphic Belt, central Shikoku, southwest Japan. Island Arc, 14, 215-235.

Miyamoto, A., Enami, M., Tsuboi, M., and Yokoyama, K. (2007) Peak conditions of kyanite-bearing quartz eclogites in the Sanbagawa metamorphic belt, central Shikoku, Japan. Journal of Mineralogical and Petrological Sciences, 102, 352-367.

Mouri, T. and Enami, M. (2008) Areal extent of eclogite facies metamorphism in the Sanbagawa belt, Japan: New evidence from a Raman microprobe study of quartz residual pressure. Geology, 36, 503-506.

Nagaya, T., Wallis, S.R., Kobayashi, H., Michibayashi, K., Mizukami, T., Seto, Y., Miyake, A., and Matsumoto, M. (2014) Dehydration breakdown of antigorite and the formation of B-type olivine CPO. Earth and Planetary Science Letters, 387, 67-76.

Novak, G.A., and Gibbs, G.V. (1971) The crystal chemistry of the silicate garnets.

American Mineralogist, 56, 791-825.

Okamoto, A., and Michibayashi, K. (2006) Misorientations of garnet aggregate within a vein; an example from the Sanbagawa metamorphic belt, Japan. Journal of Metamorphic Geology, 24, 353-366.

Ota, T., Terabayashi, M., and Katayama, I. (2004) Thermobaric structure and metamorphic evolution of the Iratsu eclogite body in the Sanbagawa belt, central Shikoku, Japan. Lithos, 73, 95-126.

Padròn-Navarta, J.A., Tommasi, A., Garrido, C.J., and Sánchez-Vizcaíno, V.L. (2012) Plastic deformation and development of antigorite crystal preferred orientation in high-pressure serpentinites. Earth and Planetary Science Letters, 349-350, 75-86.

Pattison, D.R.M. (2001) Instability of Al_2SiO_5 "triple-point" assemblages in muscovite+biotite+quartz-bearing metapelites, with implications. American Mineralogist, 86, 1414-1422.

Prior, D.J., Wheeler, J., Brenker , F.E., Harte, B., and Matthews, M. (2000) Crystal plasticity of natural garnets: new microstructural evidence. Geology, 28, 1003-1006.

Robyr, M., Vonlanthen, P., Baumgartner, L.P., and GrobetY, B. (2007) Growth mechanism of snowball garnets from the Lukmanier Pass area (Central Alps, Switzerland): a combined μCT/EPMA/EBSD study. Terra Nova, 19, 240-244.

Ruiz Cruz, M.D. (2011) Origin of atoll garnet in schists from the Alpujarride Complex (Central zone of the Betic Cordillera, Spain): Implications on the P-T evolution. Mineralogy and Petrology, 101, 245-261.

Sakurai, T., and Takasu, A. (2009) Geology and metamorphism of the Gazo mass (eclogite-bearing tectonic block) in the Sambagawa metamorphic belt, Besshi

district, central Shikoku, Japan. Journal of Geological Society of Japan, 115, 101-121 (in Japanese with English abtract).

Schertl, H.P., and Neuser, R.D. (2007) Unusual lath-shaped garnet-zoisite intergrowth textures from a UHP zoisite-quartz fels, Dora Maira, northwest Italy: An EBSD case study. International Geology Review, 49, 626-635.

Searle, M.P., Noble, S.R., Cottle, J.M., Waters, D.J., Mitchell, A.H.G., Tin Hlaing, and Horstwood, M.S.A. (2007) Tectonic evolution of the Mogok metamorphic belt, Burma (Myanmar) constrained by U-Th-Pb dating of metamorphic and magmatic rocks. Tectonics, 26, TC3014.

Spear, F.S. and Cheney, J.T. (1989) A petrogenetic grid for pelitic schists in the system SiO_2-Al_2O_3-FeO-MgO-K_2O-Na_2O-H_2O. Contributions to Mineralogy and Petrology, 101, 149-164.

Spear, F.S., Kohn, M.J., Florence, F.P., and Menard, T. (1990) A model for garnet and plagioclase growth in pelitic schists; implications for thermobarometry and P-T path determinations. Journal of Metamorphic Geology, 8, 683-696.

Spiess, R., Peruzzo, L., Prior, D.J., and Wheeler, J. (2001) Development of garnet porphyroblasts by multiple nucleation, coalescence and boundary misorientation-driven rotations. Journal of Metamorphic Geology, 19, 269-290.

Storey, C.D., and Prior, D.J. (2005) Plastic deformation and recrystallization of garnet: A mechanism to facilitate diffusion creep. Journal of Petrology, 46, 2593-1613.

Taguchi, T., and Enami, M. (2014) Compositional zoning and inclusions of garnet in Sanbagawa metapelites from the Asemi-gawa route, central Shikoku, Japan. Journal of Mineralogical and Petrological Sciences, 109, 1-12.

Takasu, A. (1984) Prograde and retrograde eclogites in the Sambagawa metamorphic

belt, Besshi district, Japan. Journal of Petrology, 25, 619-643.

Thompson, A.B., Tracy, R.J., Lyttle, P., and Thompson, J.B.J. (1977) Prograde reaction histories deduced from compositional zonation and mineral inclusions in garnet from the Gassetts schist, Vermont. American Journal of Science, 277, 1152-1167.

Vollbrecht, A., Pawlowski, J., Leiss, B., Heinrichs, T., Seidel, M., and Kronz, A. (2006) Ductile deformation of garnet in mylonitic gneisses from the Munchberg Massif (Germany). Tectonophysics, 427, 153-170.

Wallis, S., Takasu, A., Enami, M., and Tsujimori, T. (2000) Eclogite and related metamorphism in the Sanbagawa belt, Southwest Japan. Bulletin of Research Institute of Natural Sciences, Okayama University of Science, 26, 3-17.

Whitney, D.L., and Evans, B.W. (2010) Abbreviations for names of rock–forming minerals. American Mineralogist, 95, 185-187.

Whitney, D.L., Goergen, E.T., Ketcham, R.A., and Kunze, K. (2008) Formation of garnet polycrystals during metamorphic crystallization. Journal of Metamorphic Geology, 26, 365-383.

Whitney, D.L. and Seaton, N.C.A. (2010) Garnet polycrystals and the significance of clustered crystallization. Contributions to Mineralogy and Petrology, 160, 591-607.

Wu, C.-M., Zhang, J., and Ren, L.-D. (2004) Empirical garnet–biotite–plagioclase–quartz (GBPQ) geobarometry in medium- to high-grade metapelites. Journal of Petrology, 45, 1907-1921.

Ye Kyaw Thu, Maw Maw Win, Enami, M., and Tsuboi, M. (2016: in press) Ti-rich biotite in spinel and quartz-bearing paragneiss and related rocks from the Mogok metamorphic belt, central Myanmar. Journal of Mineralogical and Petrological

Sciences, 111, doi: 10.2465/jmps.151020.

Zaw Win Ko, Enami, M., and Aoya, M. (2005) Chloritoid and barroisite-bearing pelitic schists from the eclogite unit in the Besshi district, Sanbagawa metamorphic belt. Lithos, 81, 79-100.

Figure captions

FIGURE 1. (a) Schematic diagram showing the pressure–temperature paths of composite- and normal-zoned garnets in metapelites collected from eclogite and non-eclogite units of the Besshi region in the Sanbagawa belt [partly modified from Fig. 11b of Kouketsu et al. (2014a)]. (b) Pressure and temperature estimations of the Mogok metamorphic rocks from the Sagaing area, central Myanmar. Abbreviations are: And, andalusite; Ky, kyanite; Sil, sillimanite; M16, Maw Maw Win (2016). Stability ranges of aluminum silicates are from Pattison (2001).

FIGURE 2. (a) Photomicrograph and (b) CaKα, (c) MgKα, (d) FeKα, and (e) and (f) MnKα X-ray mapping images of a garnet in the Sanbagawa metapelite sample (UKE07b). In the X-ray mapping images, warmer colors indicate high concentrations of elements. The white lines in Fig. 2b correspond to the domain boundaries shown in Fig. 4a determined by EBSD analysis, and that in Fig. 2e indicates outline of garnet. Line A–B indicates the position of the step-scan analysis shown in Fig. 3.

FIGURE 3. Step-scan analysis of a garnet in the Sanbagawa metapelite sample (UKE07b). The position of the step-scan is shown in Fig. 2a. Abbreviations for end-members: Alm: almandine; Grs: grossular; Prp: pyrope; Sps: spessartine.

FIGURE 4. Four-domain garnet polycrystals containing quartz inclusions in the Sanbagawa metapelite sample (UKE07b). (a) Electron backscatter diffraction (EBSD) map (6 μm grid step) showing the relationships of crystallographic orientations of garnet domains and quartz inclusions. Average crystallographic orientations of quartz inclusions are indicated by colored circles corresponding to

the Euler angle color key. (b) Equal-area and lower hemisphere projection showing average crystallographic orientations of garnet domains. The Euler angle color keys and band contrast are shown in (a). (c) Equal-area and lower hemisphere projections showing average crystallographic orientations of quartz grains included in the garnet shown in (a). The Euler angle color keys of the poles are the same as those of the quartz inclusions shown in (a).

FIGURE 5. Relationships of crystallographic orientations of sets of quartz grains [(1)–(3), (4)–(5), and (6)–(7)] included in the neighboring garnet domains in the Sanbagawa metapelite sample (UKE07b) shown in Fig. 4a. (a) and (c) Electron backscatter diffraction (EBSD) maps (1 μm grid step) of quartz inclusions and host garnet. The mapped areas are shown in Figs. 2f and 4a. The different colors, which correspond to the Euler angle color key, denote different orientations of quartz and garnet. (b) and (d) Equal-area and lower hemisphere projections showing average crystallographic orientations of quartz grains. The Euler angle color keys of (b) and (d) are shown in (a) and (c), respectively. Areas A–D are domain boundaries analyzed by EPMA; their compositions are shown in Fig. 9. Abbreviations for minerals: Grt, garnet; Qz, quartz.

FIGURE 6. (a) Photomicrograph, (b) and (d) MgKα, and (c) and (e) MnKα X-ray images of sets of garnet segments in the Mogok pelitic gneiss sample (S22b). In the X-ray map images, warmer colors indicate high concentrations of elements. Line C–D indicates the position of the step-scan analysis shown in Fig. 7. Abbreviations for minerals: Bt: biotite; Grt: garnet; Pl: plagioclase; Qz: quartz.

FIGURE 7. Step-scan analysis of a garnet in the Mogok pelitic gneiss sample (S22b). The position of the step-scan is shown in Fig. 6a. Abbreviations for end-

members: Alm: almandine; Grs: grossular; Prp: pyrope; Sps: spessartine.

FIGURE 8. Sets of garnet segments in the Mogok pelitic gneiss sample (S22b). (a) and (d) Electron backscatter diffraction (EBSD) maps (10 μm grid step) showing similarities and differences in the lattice orientations of the garnet segments. Different colors denote different orientations. (b), (c), and (e) Equal-area and lower hemisphere projections showing average crystallographic orientations of all segments in each figure.

FIGURE 9. Compositional variations of a garnet in the Sanbagawa metapelite sample (UKE07b). The positions of areas A–D of the segment boundary are shown in Figs. 5a and c.

FIGURE 10. Conceptual diagram of the garnet nucleation and growth scenario of garnet polycrystals in the Sanbagawa metapelite (UKE07b). The growth of this grain began in the initial formations of closely spaced nuclei followed by their coalescence during the early stage of prograde eclogite facies metamorphism. At that time, some of the quartz grains were included at the domain boundaries.

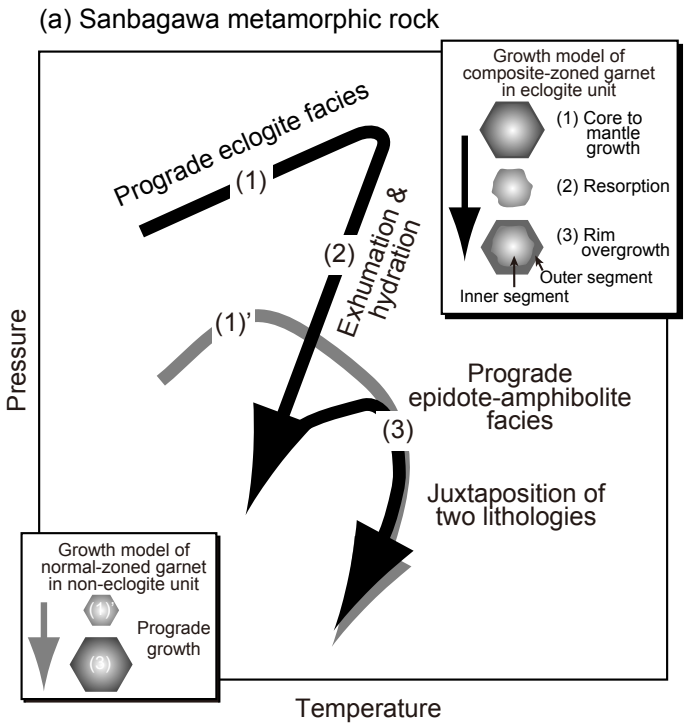

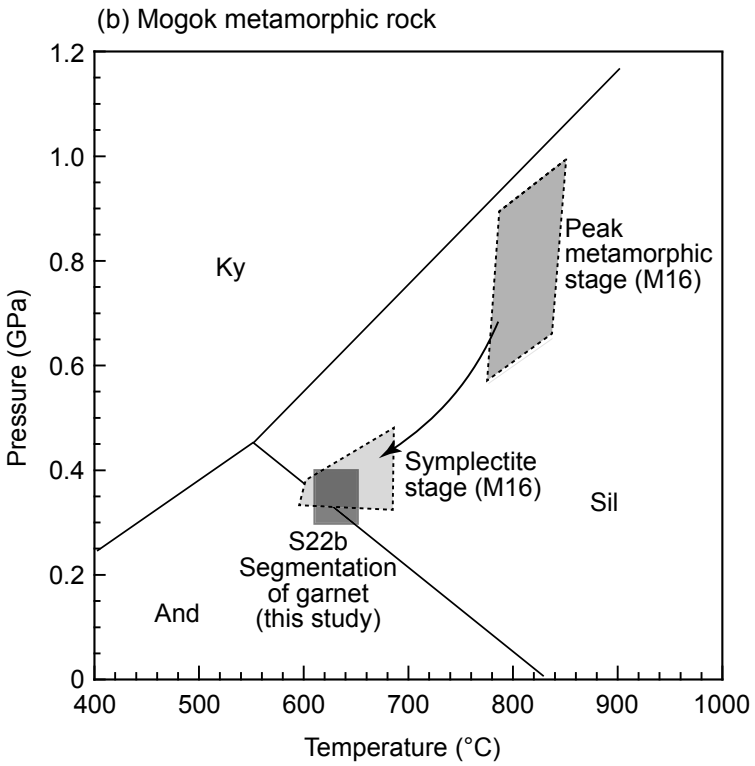

Figure 01 (Enami and others)

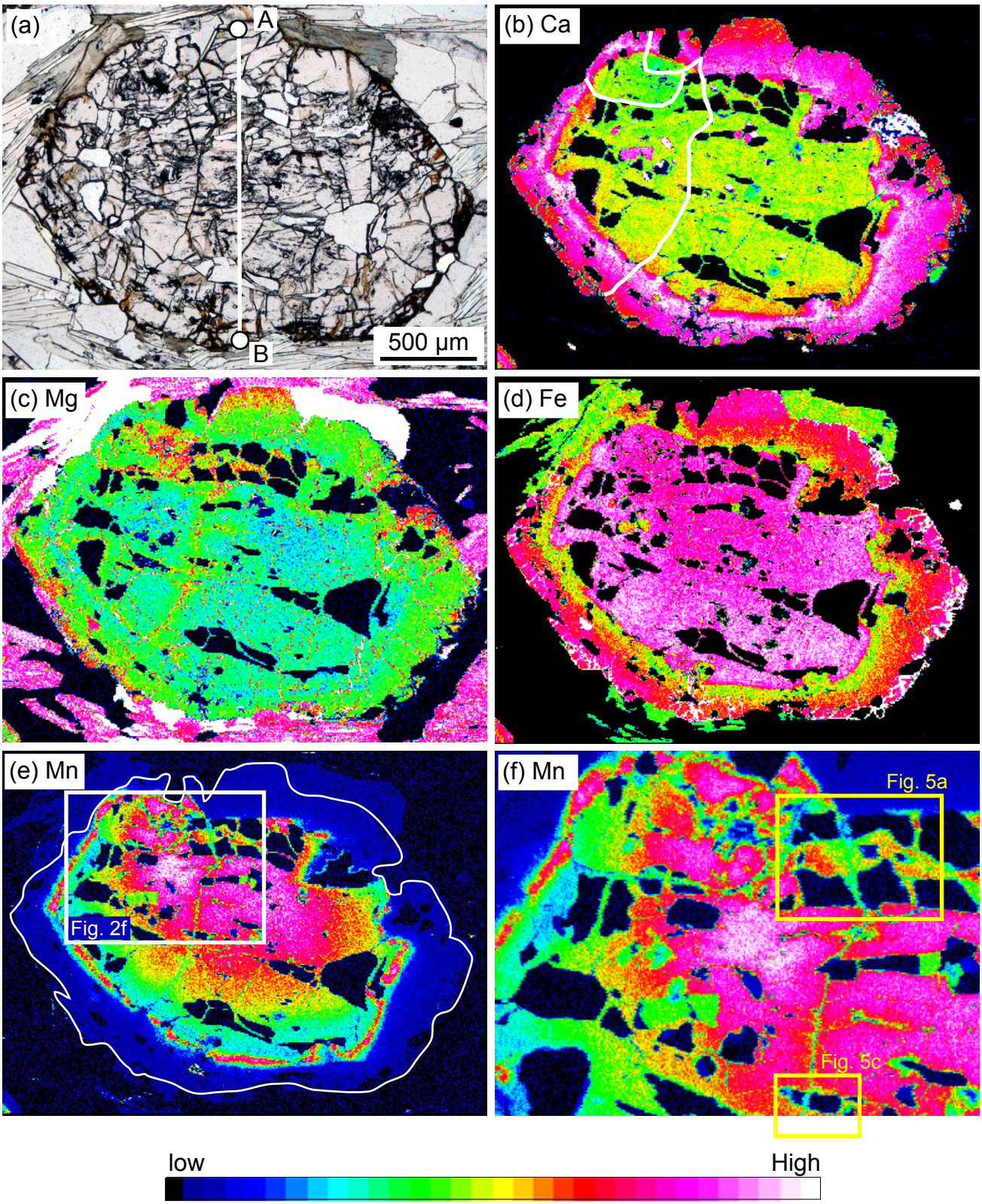

Figure 02 (Enami and others)

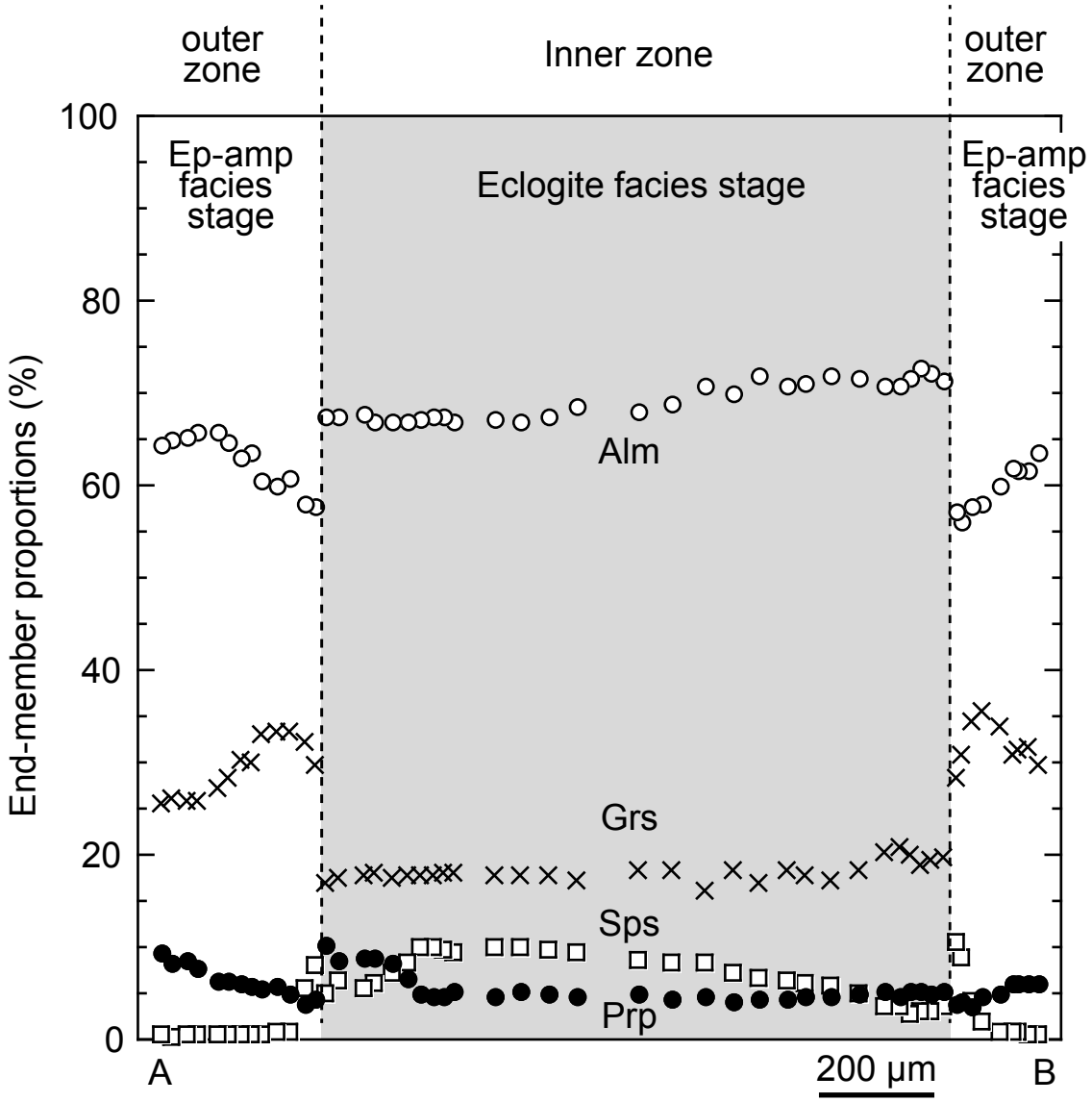

Figure 03 (Enami and others9

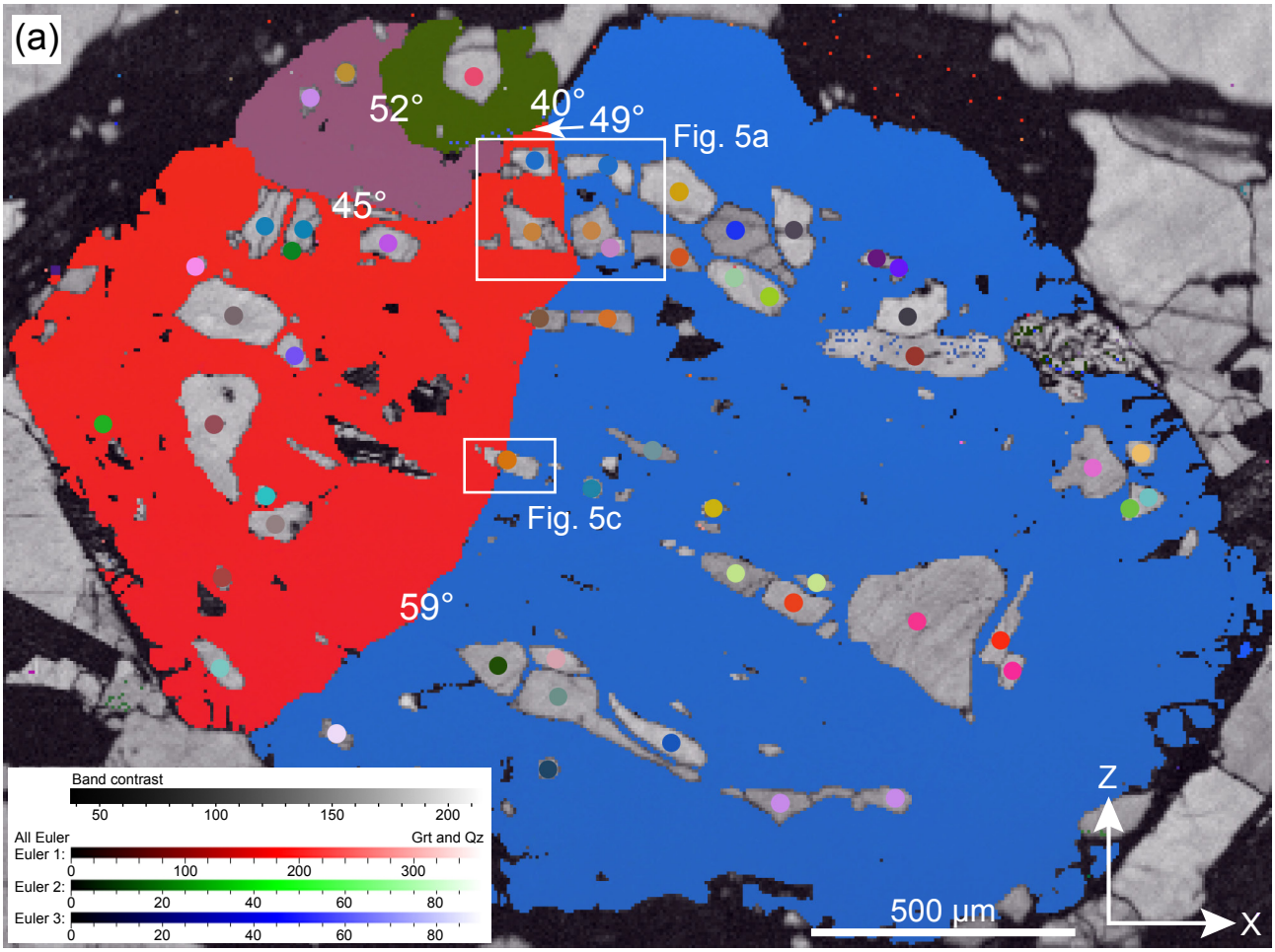

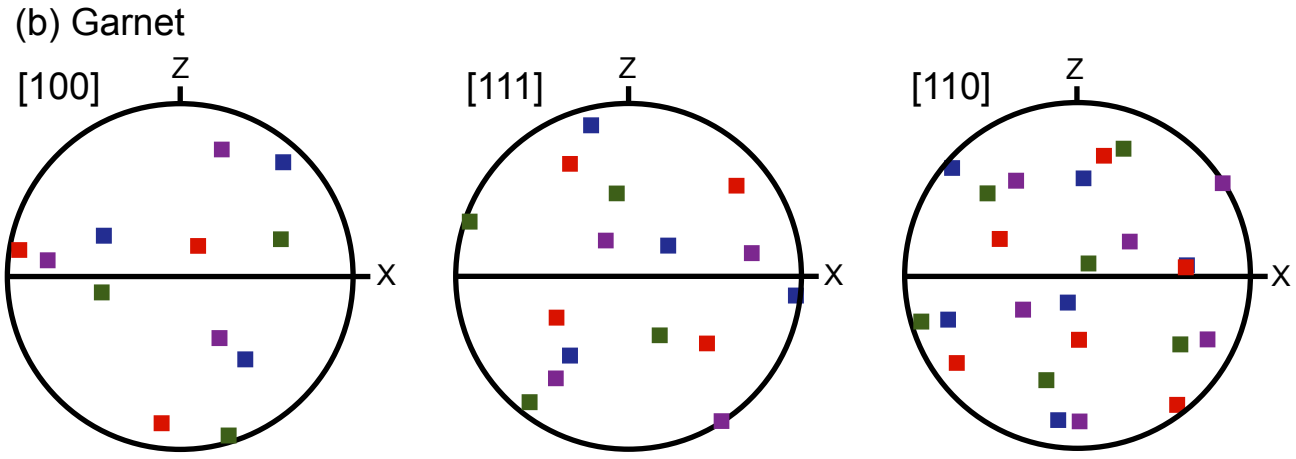

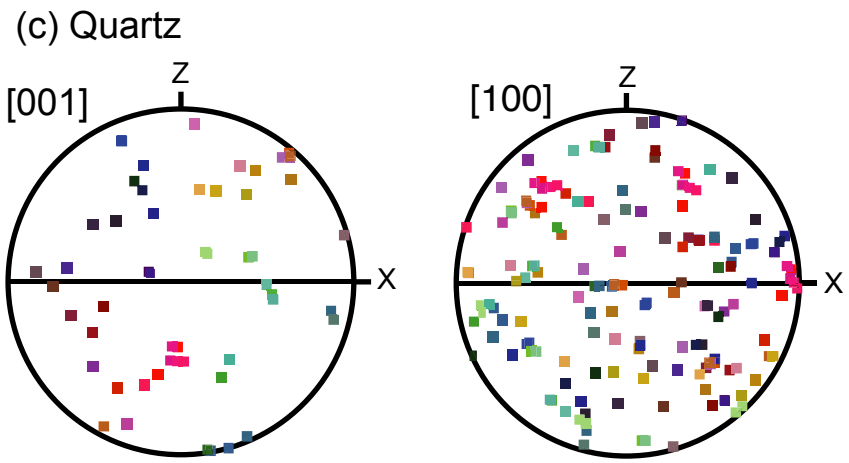

Figure 04 (Enami and others)

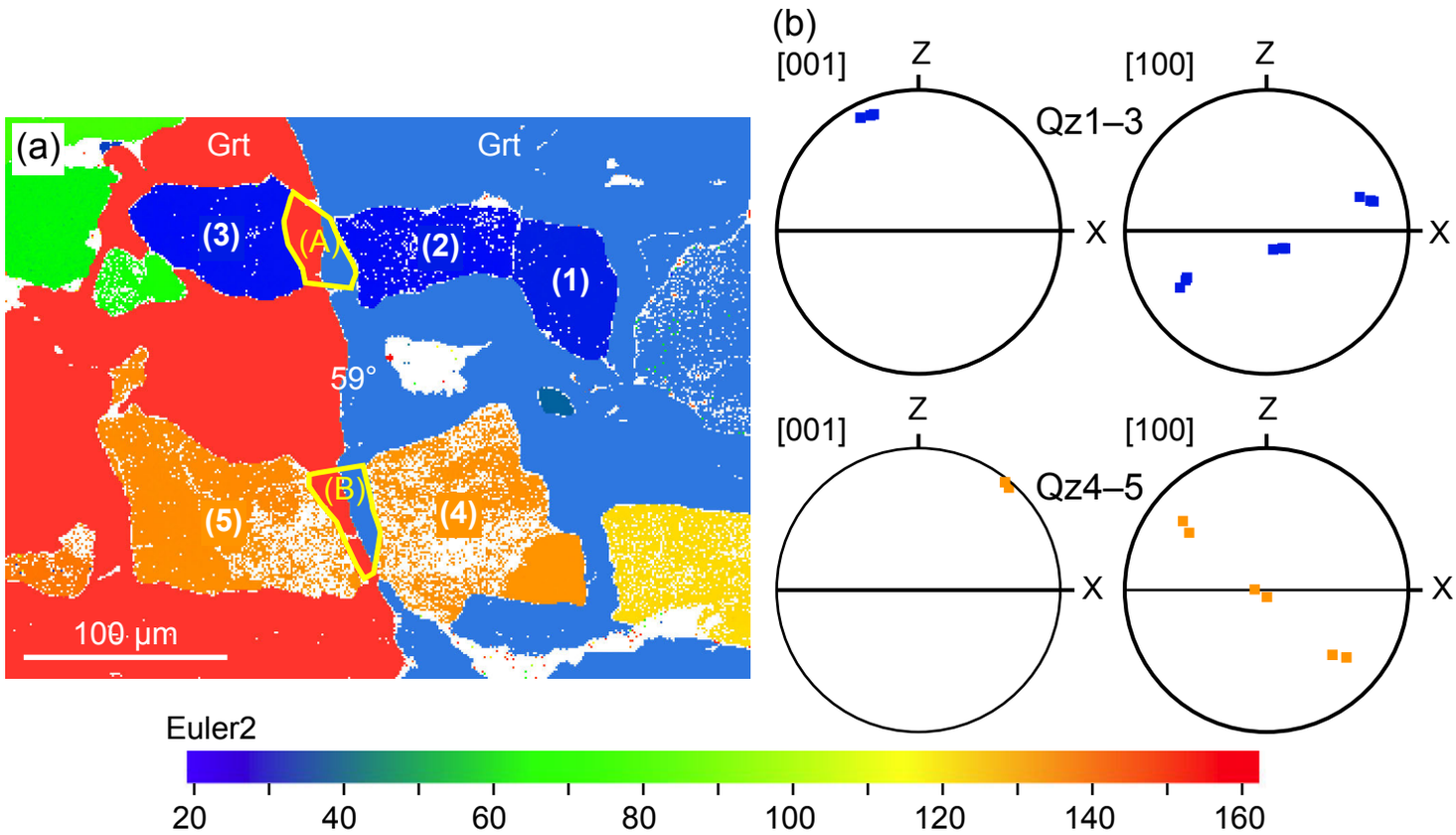

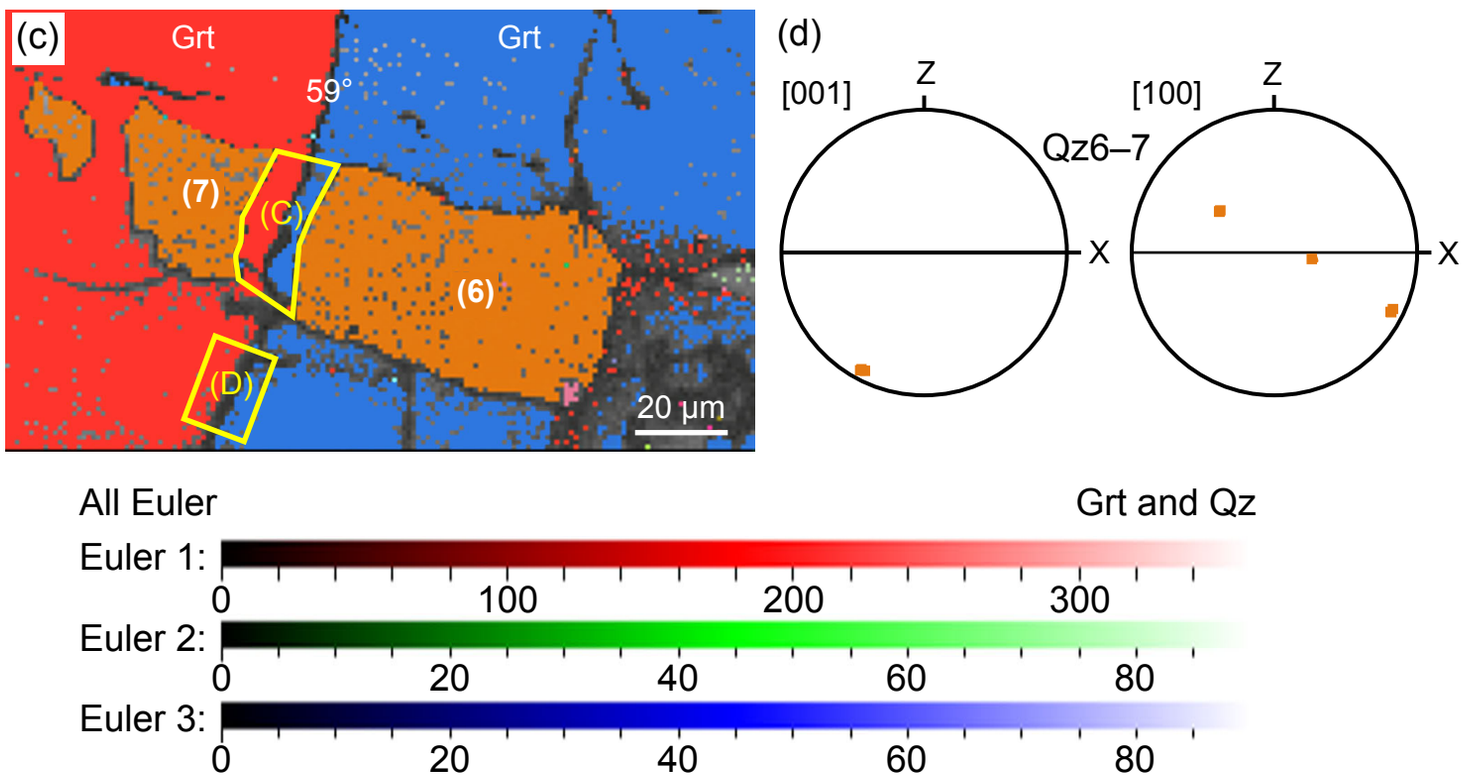

Figure 05 (Enami and others)

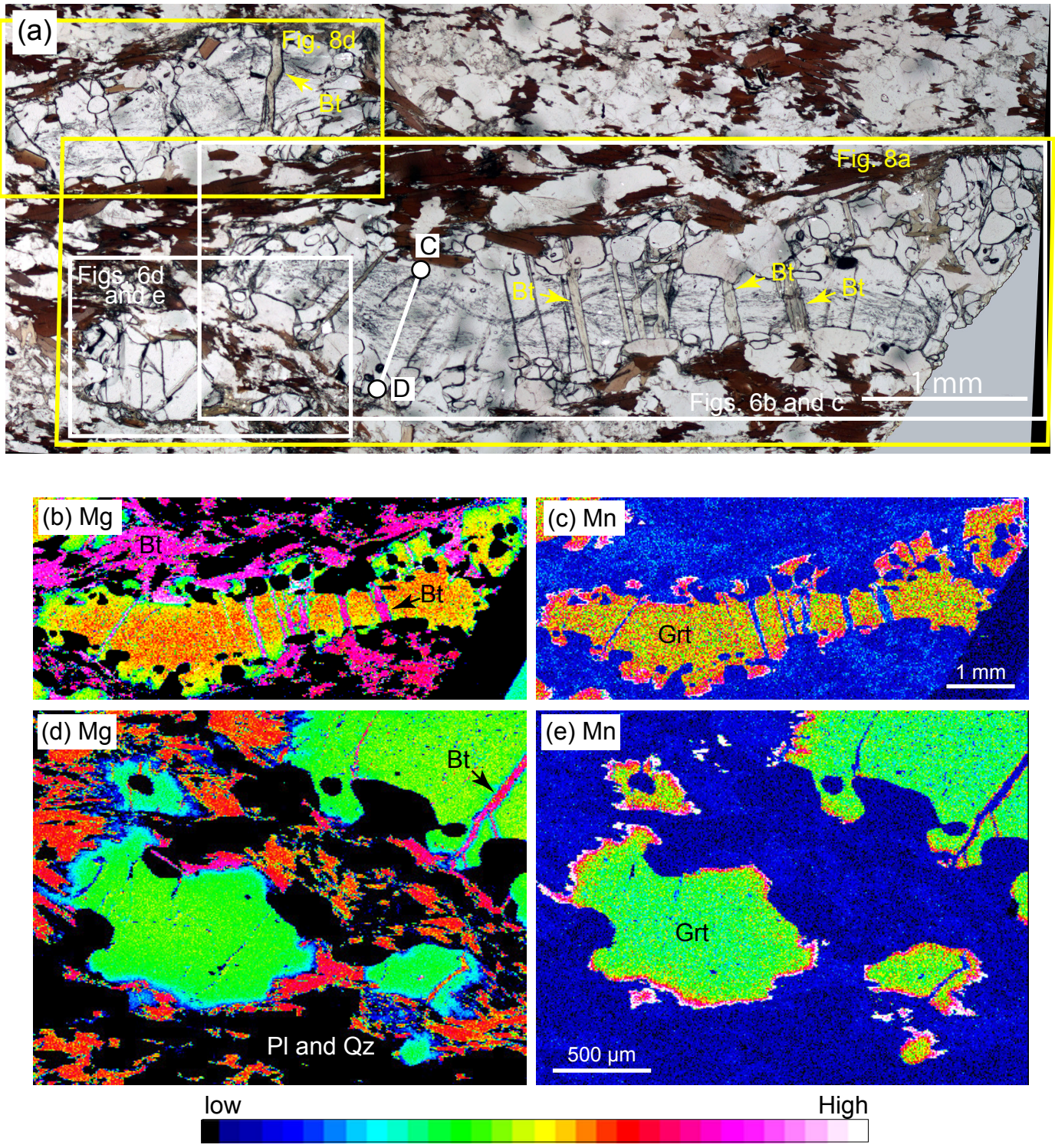

Figure 06 (Enami and others)

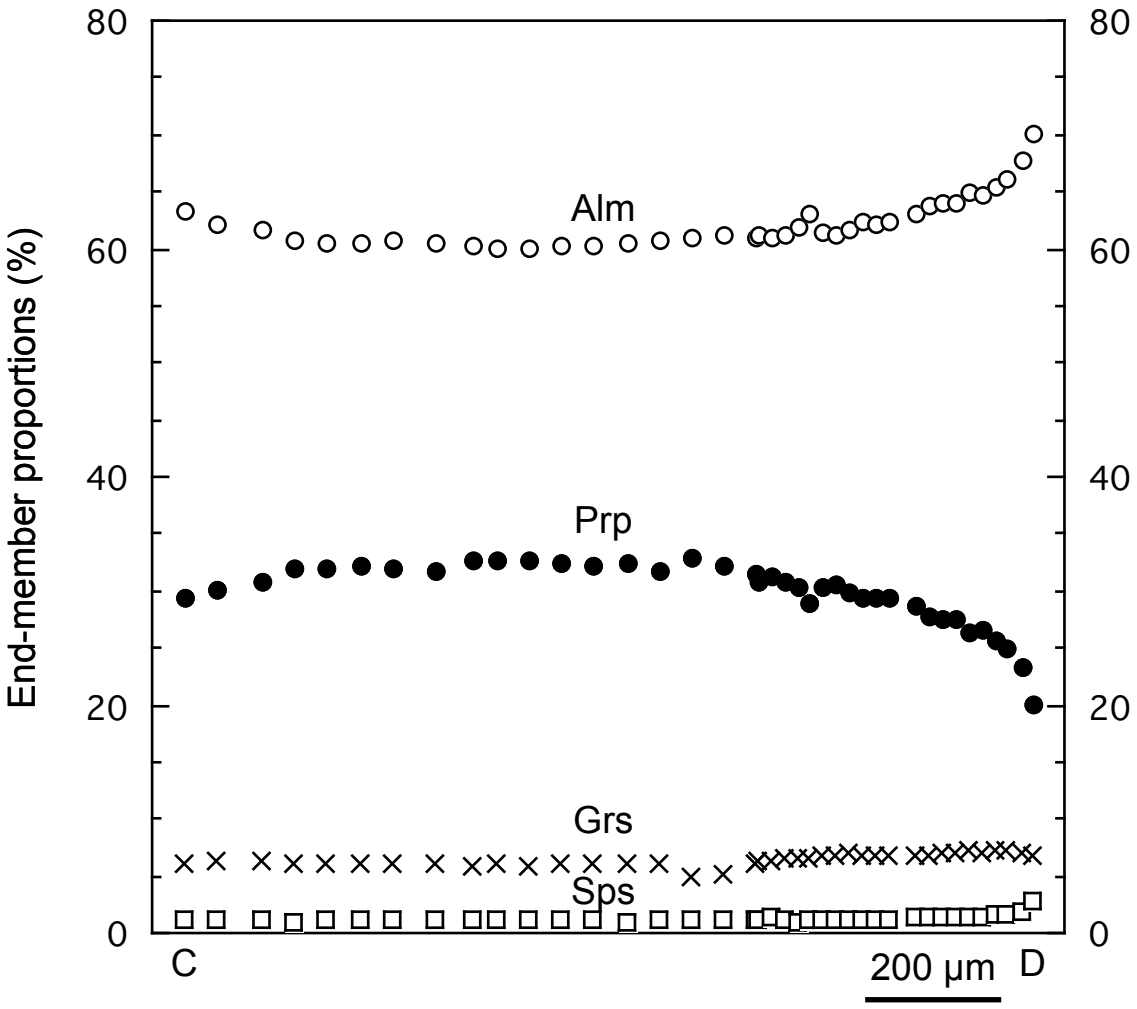

Figure 07 (Enami and others)

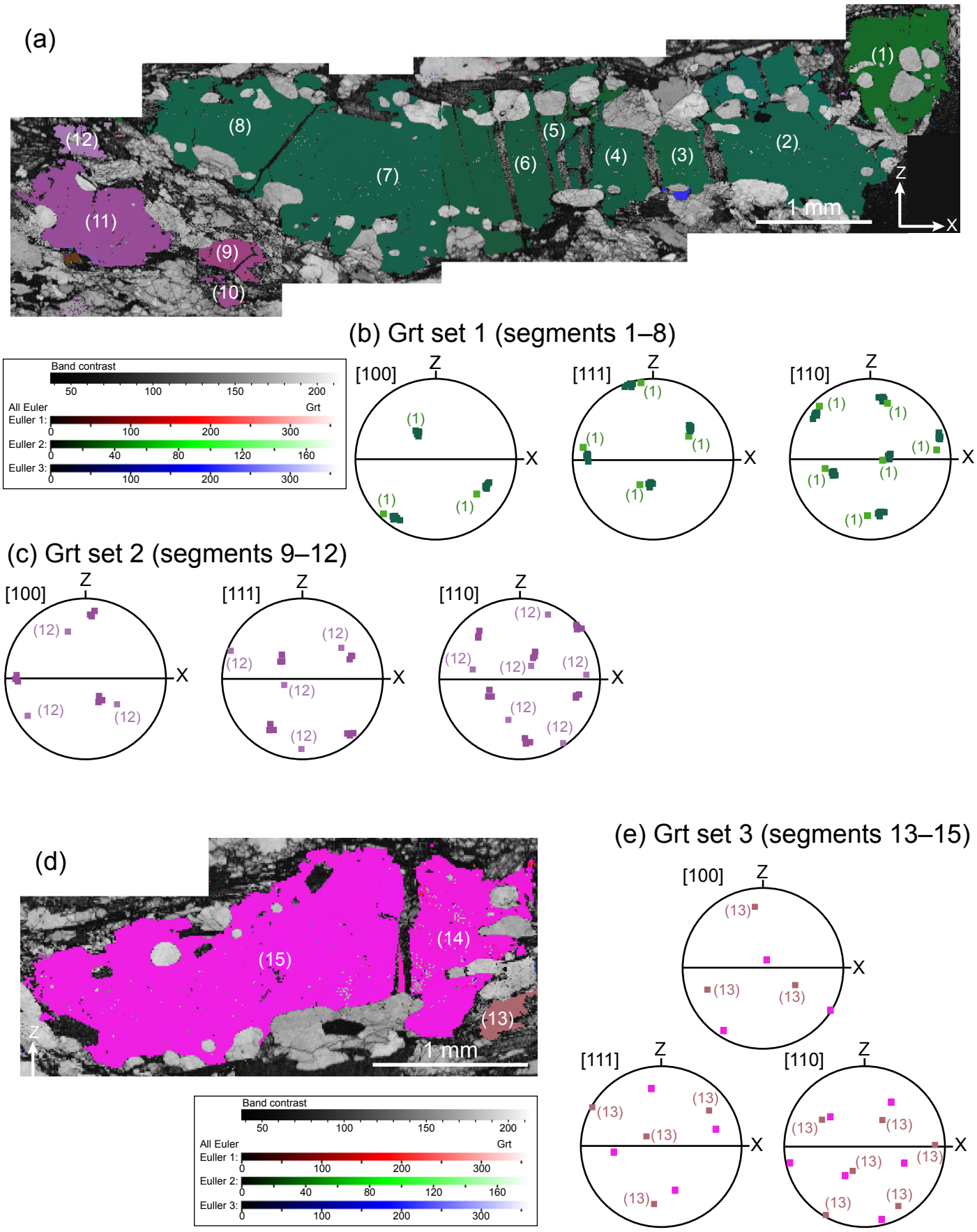

Figure 08 (Enami and others)

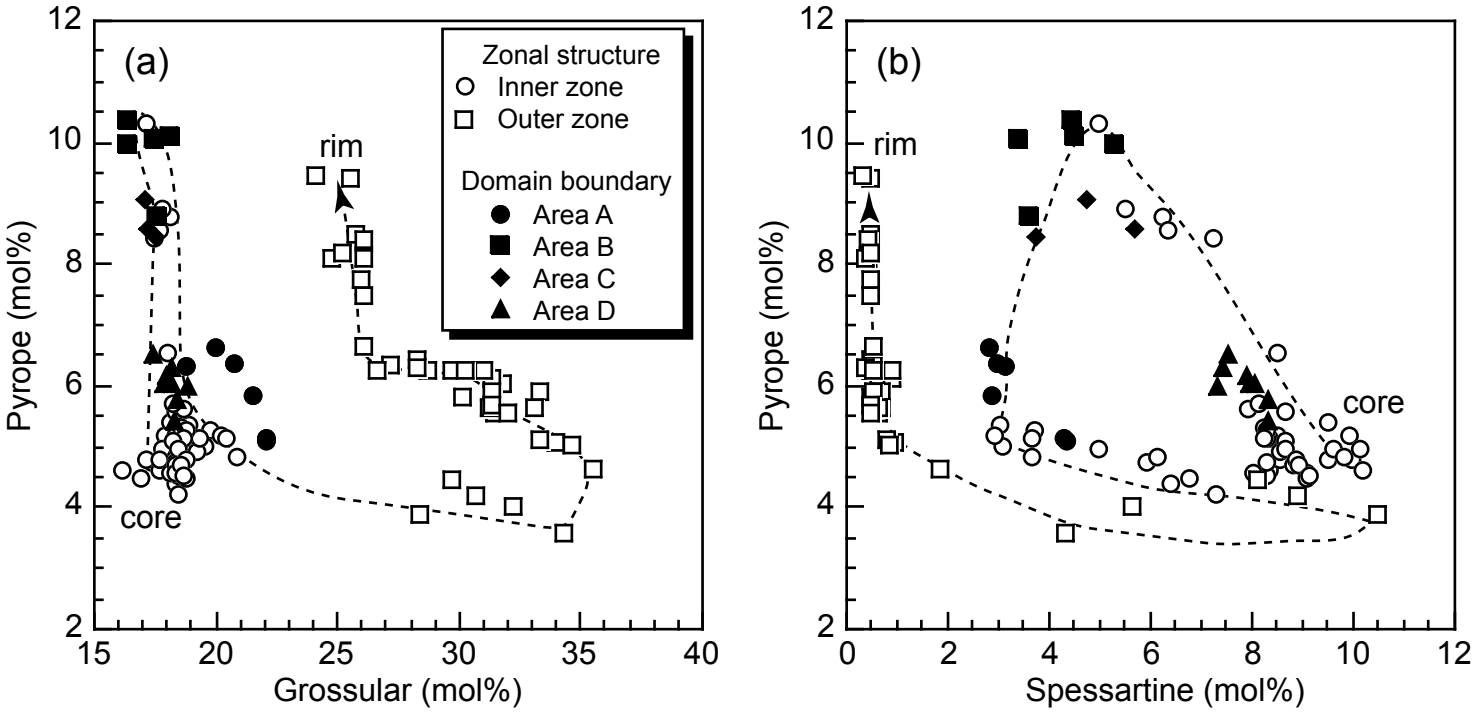

Figure 09 (Enami and others)

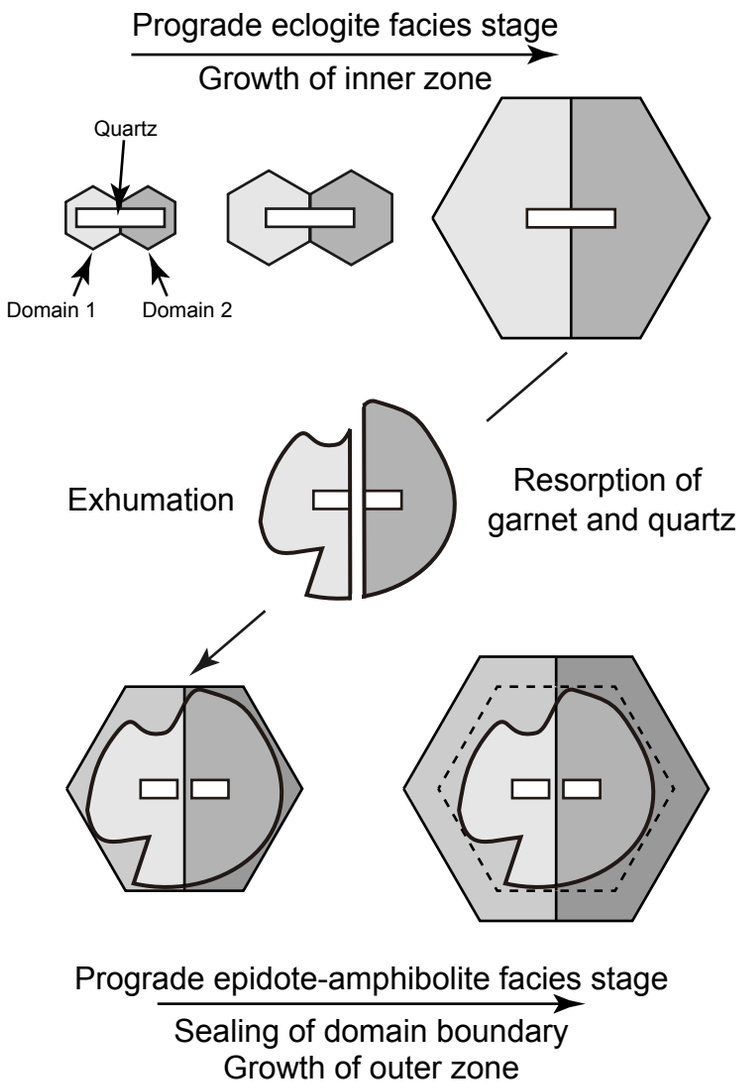

Figure 10 (Enami and others)

SUPPLEMENTAL TABLE 1. Representative chemical compositions of major minerals in the Sanbagawa metapelite and Mogok pelitic gneiss.

	UKE07b							S22b				
	Garnet				Amp	Pg	Phn	Garnet		Biotite		Pl
	I (c)	I (m)	O (i)	O (r)				core	rim	Iso	mo	mo
SiO_2	37.24	37.16	37.50	37.49	46.07	47.29	51.15	38.40	37.60	37.10	36.88	56.97
TiO_2	0.09	0.06	0.11	0.08	0.34	0.06	0.25	0.04	0.05	4.89	2.95	0.03
Al_2O_3	21.00	21.11	20.97	21.10	14.40	39.81	27.85	21.60	21.10	17.85	19.22	27.26
FeO*	31.30	30.82	26.39	29.81	13.15	0.74	2.18	29.24	34.07	15.10	16.28	0.04
MnO	3.35	2.23	3.65	0.22	0.05	0.00	0.02	0.56	1.00	0.05	0.00	0.02
MgO	1.56	2.64	1.15	2.44	10.78	0.19	3.26	8.84	5.23	11.06	10.96	0.01
BaO										0.16	0.00	0.01
CaO	6.78	6.08	10.58	9.18	8.65	0.12	0.01	2.10	1.32	0.01	0.03	8.95
Na_2O					3.65	7.82	0.58	0.00	0.02	0.15	0.14	6.30
K_2O					0.49	0.27	10.29	0.00	0.00	9.87	9.73	0.14
Total	101.32	100.10	100.35	100.32	97.58	96.30	95.59	100.78	100.39	96.24	96.19	99.73
O	12	12	12	12	23	11	11	12	12	11	11	8
Si	2.972	2.976	2.991	2.980	6.692	2.992	3.395	2.965	2.985	2.741	2.732	2.560
Ti	0.005	0.004	0.007	0.005	0.037	0.003	0.012	0.002	0.003	0.272	0.164	0.001
Al	1.975	1.992	1.971	1.976	2.465	2.969	2.178	1.966	1.974	1.554	1.678	1.444
Fe*	2.089	2.064	1.760	1.981	1.597	0.039	0.121	1.888	2.262	0.939	1.009	0.002
Mn	0.226	0.151	0.247	0.015	0.006	0.00	0.001	0.037	0.067	0.003	0.000	0.001
Mg	0.186	0.315	0.137	0.289	2.334	0.018	0.322	1.017	0.619	1.218	1.210	0.001
Ba										0.005	0.000	0.000
Ca	0.580	0.522	0.904	0.782	1.346	0.008	0.001	0.174	0.112	0.001	0.002	0.431
Na					1.028	0.959	0.075	0.000	0.003	0.021	0.020	0.549
K					0.091	0.022	0.871	0.000	0.000	0.930	0.919	0.008

* Total iron as FeO.
Abbreviations are: I (c), core of inner zone; I (o), margin of inner zone;
O (i), inner part of outer zone; O (r), rim of outer zone; Iso, isolated grain in matrix;
mo, mosaic aggregate;